Powder Technology 206 (2011) 122–131

Contents lists available at ScienceDirect

Powder Technology

journal homepage: www.elsevier.com/locate/powtec

Analysis of the product granulometry, temperature and mass flow of an industrial multichamber fluidized bed urea granulator

Diego E. Bertin *, Ivana M. Cotabarren, Verónica Bucalá, Juliana Piña

Department of Chemical Engineering, Universidad Nacional del Sur, PLAPIQUI, CONICET, Camino La Carrindanga Km. 7, (8000) Bahía Blanca, Argentina

ARTICLE INFO

Available online 25 June 2010

Keywords:
Granulation
Industrial multichamber fluidized bed granulator
Population balance modeling
Product granulometry

ABSTRACT

In this work, a complete dynamic model of a continuous industrial fluidized bed granulator for urea production is presented. Three growth and three cooling chambers in series are simulated. Mass, energy and momentum balances are solved for all the fluidized beds together with the population balance equation (PBE). Since each granulator chamber can be modelled as a continuous stirred tank (CST), the multichamber granulator is represented by a series of CSTs.

Applying the developed model, the open-loop behaviour of the product granulometry is particularly investigated. With this aim, and to further develop efficient control strategies, different step disturbances are assayed. Based on the results of the performed sensitivity study, it can be concluded that the log-normal distribution function gives an appropriate description of the PSD in each chamber, the granulometry response times control the dynamics of the complete granulation circuit, the seeds' PSD is the variable that most affect the outlet particle size distribution, and that mild recycle ratio values are adequate to stabilize the granulator operation.

1. Introduction

Within the wide variety of industries that utilize granulation to produce particles with defined properties, the fertilizer manufacture has an essential role in securing food supplies around the world. Urea is one of the most often used nitrogen-based fertilizers, being marketed as prills or granules. The last form is the preferred route of production, since the particles are larger, harder, and more resistant to moisture than prills. As a result, urea in granular form has become a more suitable material for fertilizer blends [1].

After several years of extraordinary growth, the world economy is entering a depressed period. Even though, the situation deteriorated quickly during the third quarter of 2008, the nitrogenous fertilizers demand should not be greatly affected. In 2008, the global urea capacity was estimated at 163 Mt. In 2009, the global urea capacity is projected to increase by 11 Mt, to 174 Mt [2]. There are many urea granulation plants in operation around the world and some under construction. However, the current tight market conditions for fertilizers may lead to the closure of uncompetitive plants. In this context, knowledge improvements to operate more efficiently urea granulation plants are extremely worthy.

The heart of the urea granulation circuit is the granulator, which for many technologies is a fluidized bed unit [3–5]. This unit generally has several growth chambers, each one is basically a bed of solids fluidized by air where relatively small urea granules (called seeds) are fed continuously and a urea concentrated liquid solution is sprayed from the bottom of the unit. The granules grow through deposition of the tiny liquid drops onto the seeds, followed mainly by the urea solidification. The growing particles flow under-currently from one chamber to another. Cooling chambers, where no urea solution is supplied, are often placed downstream the growth beds to meet specific requirements for further processing of the granules [6].

The urea granules must fulfil certain quality parameters in order to be suitable for commercialization: adequate mean diameter and a relatively narrow particle size distribution (PSD) to avoid segregation and facilitate its application on soils. Usually a relatively low mass fraction of the granules leaving the granulator has the marketable product granulometry. Hence classification and crusher units are required downstream the granulator to condition the out of specification product that is recycled to the granulation unit as seeds. For this reason, the granulator product PSD strongly affects the recycle ratio and consequently the granulation circuit stability.

Currently, the industrial urea fluidized bed granulators are usually operated by trial and error [3,7,8]. The dynamics of these units is not easy to be predicted, this makes difficult to run the plants at steady-state or even to operate for relatively long times (e.g. one month) without undesired shut downs (e.g. caused by dry/wet quenching, grid blinding, etc. [9]). Therefore, it is important to understand more deeply the granulator behaviour in order to develop rational tools for maximizing the plant profit (i.e. increasing the production rates and limiting the undesired shut downs) while simultaneously obtaining a marketable product (i.e., of suitable granulometry).

* Corresponding author.
E-mail address: dbertin@plapiqui.edu.ar (D.E. Bertin).

0032-5910/$ – see front matter © 2010 Elsevier B.V. All rights reserved.
doi:10.1016/j.powtec.2010.06.016

Bertín et al. [10,11] analyzed the unsteady-state operation of a fluidized bed urea granulator and compared the simulation predictions of the operating variables against industrial data. For those studies, the authors assumed that the particles' population could be represented by a number-volume mean diameter. Even though the hypothesis was accurate to predict the bed temperatures, the estimation of the particle size distribution (PSD) at the granulator outlet is necessary to improve the operation of this device and of the granulation circuit, which have complex dynamics. Aiming to have a complete model to represent multichamber fluidized bed urea granulators, in this work a more detailed description of these units is presented. The conventional unsteady-state mass, energy and momentum balances are coupled with the Population Balance Equation (PBE) and simultaneously solved for several interacting fluidized beds connected in series. The sensitivity of the PSD dynamics within each chamber against disturbances in different key granulator variables is analyzed.

2. Mathematical model

Fig. 1 shows a simplified schematic representation of a typical continuous industrial granulator. As it was aforementioned, this unit is generally constituted by several fluidized chambers for growth and cooling. Urea seeds are continuously fed to the first growth chamber. The size enlargement occurs by coating of the particles surface with tiny droplets of the concentrated urea solution (usually 95 wt.%, [6]), which are atomized from the bottom of the unit by means of numerous binary spray nozzles. The solidification of the droplets on the solid particles surface takes place by cooling and water evaporation. Usually several growth chambers are used to shift the particles residence time distribution towards that of plug flow, and thus to obtain narrower particle size distributions [12,13]. The growing particles flow under-currently from one chamber to another. In the cooling chambers no urea solution is supplied and therefore no growth takes place [6]. The purpose of these last chambers is to cool down the solids to temperatures lower than those reached in the growth chambers.

Considering the unit features abovementioned and previous simulation results on the steady and unsteady-state operations of multichamber granulators [10,11,14], the model of the industrial fluidized bed urea granulator is formulated on the basis of the following assumptions:

1) The gaseous and liquid phases operate at pseudo-steady-state. Thus, the mass and energy accumulations of air and liquid within the fluidized chambers are neglected [16].
2) The solid phase is perfectly mixed.
3) The urea granules which have constant density and porosity, are spherical and free of additives such as formaldehyde.
4) All the urea melt droplets reach the solids' surface. The sprayed droplets are distributed proportionally to the fraction of total particles superficial area [3,15].
5) The elutriation of fines, formation of nuclei by attrition, breakage and/or overspray are negligible. According to industrial experimental evidence, the agglomeration of particles is insignificant.
6) The seeds are virtually dry; the water content is lower than 0.25 wt.% [6].
7) The water content of the urea melt droplets is instantaneously and completely evaporated [14].
8) Due to the intense mixing provided by the fluidization, the air and solid temperatures within each chamber are equal [14].
9) The product discharge is non-classified.

2.1. Mass, energy and momentum balances

2.1.1. Mass balances

The unsteady-state urea mass balance for a chamber k is written as:

$$\frac{dm_T^k}{dt} = \dot{m}_{in}^k + \dot{m}_{melt}^k\left(1 - x_{melt}^k\right) - \dot{m}_{out}^k \tag{1}$$

where m_T^k, $\dot{m}_{in}^k$ and $\dot{m}_{out}^k$ are the solid mass holdup, inlet and outlet particles mass flowrates, respectively. Due to the series configuration, $\dot{m}_{in}^k = \dot{m}_{out}^{k-1}$ for k from 2 to 6. $\dot{m}_{in}^1$ represents the seeds' mass flowrate to the first growth chamber, while $\dot{m}_{melt}^k$ and x_{melt}^k are the urea solution mass flowrate atomized into chamber k and its water mass fraction, respectively. Considering that the granulator has three growth chambers and three cooling compartments, $\dot{m}_{melt}^k = 0$ for chambers 4 to 6.

The mass balances are solved together with the following initial conditions:

$$m_T^k(0) = m_{T0}^k \,. \tag{2}$$

The particles flow between chambers is proportional to the square root of the pressure drop through the under-current passage area. The outlet solids mass flowrates are obtained by applying the Bernoulli equation [17]:

$$\dot{m}_{out}^k = C_D A_o^k \sqrt{2\,g\,\rho_{bed}^k\left(\rho_{bed}^k L^k - \rho_{bed}^{k+1} L^{k+1}\right)} \quad k = 1 \text{ to } 5 \tag{3}$$

$$\dot{m}_{out}^6 = C_D A_o^6 \rho_{bed}^6 \sqrt{2\,g\,L^6} \tag{4}$$

where A_0^k and L^k are the passage area and fluidized bed height of chamber k, respectively. C_D is the discharge coefficient. According to

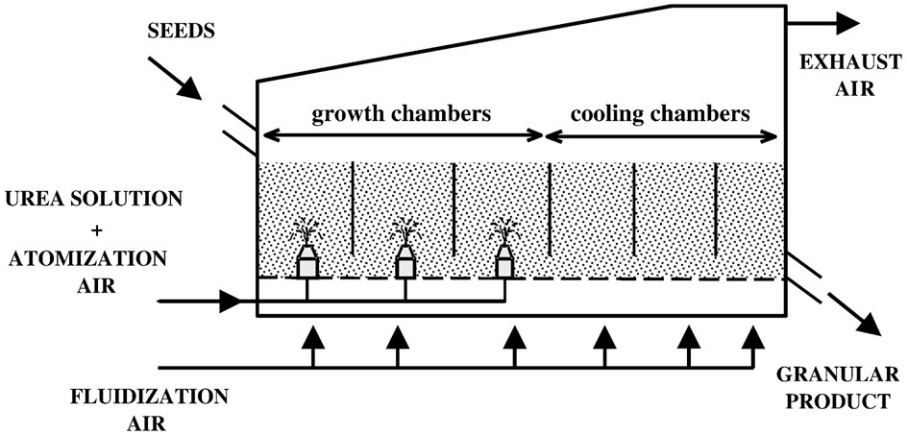

Fig. 1. Schematic representation of an industrial fluidized bed granulator for urea production.

Massimilla [18], C_D takes values around 0.5 for particles much smaller than the passage or discharge areas. ρ_{bed}^k is the bed density, defined as:

$$\rho_{bed}^k = \rho_p\left(1-\varepsilon^k\right) + \rho_a^k\,\varepsilon^k \tag{5}$$

being ρ_p and ρ_a^k the particle density and the fluidization air density in chamber k, respectively. The bed porosity ε^k is within the range delimited by the porosity at minimum fluidization conditions ε_{mf}^k and 1 (maximum porosity for complete elutriation). ε^k is estimated by the following correlation [15]:

$$\varepsilon^k = \varepsilon_{mf}^k\left(\frac{u^k}{u_{mf}^k}\right)^{K_\varepsilon} \tag{6}$$

where u^k and u_{mf}^k are the operating and minimum superficial fluidization air velocities for chamber k, respectively. The exponent K_ε is defined as follows [15]:

$$K_\varepsilon = \frac{\ln {}^{1}\!/_{\varepsilon_{mf}^k}}{\ln {}^{u_t^k}\!/_{u_{mf}^k}} \tag{7}$$

where u_t^k represents the terminal velocity.

The fluidized bed height within each chamber is calculated as:

$$L^k = \frac{m_T^k}{\rho_p A_T^k\left(1-\varepsilon^k\right)} \tag{8}$$

being A_T^k the cross sectional area of chamber k.

2.1.2. Energy balances

The following non steady-state energy balance is considered to compute the temperature T^k in each chamber [10,11]:

$$\begin{aligned} m_T^k\, cp_u(T^k)\frac{dT^k}{dt} &= \dot{m}_{in}^k \int_{T^{k-1}}^{T^k} cp_u dT + \dot{m}_{melt}^k\left(1-x_{melt}^k\right)\int_{T_{melt}^k}^{T^k} cp_u dT + \dot{m}_{melt}^k x_{melt}^k \int_{T_{melt}^k}^{T^k} cp_w dT \\ &\quad - \dot{m}_{melt}^k x_{melt}^k \Delta H_{EV}(T^k) + \dot{m}_{melt}^k\left(1-x_{melt}^k\right)\Delta H_{DIS}(T_{melt}^k) + \dot{m}_a^k \int_{T_a^k}^{T^k} cp_a dT \\ &\quad + \dot{m}_a^k Y^k \int_{T_a^k}^{T^k} cp_v dT \end{aligned} \tag{9}$$

where T_{melt}^k, T_a^k and T^{k-1} are the temperatures of the melt, fluidization air and solids entering to chamber k, respectively. T^k is the chamber temperature, ΔH_{DIS} and ΔH_{EV} are the latent heats associated to the urea melt dissolution and water evaporation. cp_u, cp_w, cp_a and cp_v are the mass heat capacities of the solid urea, liquid water, air and water vapor, respectively.

The next initial conditions are required to solve Eq. 9:

$$T^k(0) = T_0^k \tag{10}$$

According to previous works [14], the relatively low water content of the urea solution (5 wt.%) is completely evaporated, therefore the vapor flowrate is equal to the water liquid loading [19,20].

$$\dot{m}_{EV} = \dot{m}_{melt}^k x_{melt}^k \tag{11}$$

The urea physical properties used to solve the proposed dynamic model can be found elsewhere [14,21,22].

2.1.3. Momentum balances

The total pressure drop in each chamber is constituted by two terms that take into account the fluidized bed weight and air distributor pressure drop:

$$\Delta P_T^k = \Delta P_{bed}^k + \Delta P_{dist}^k = \rho_{bed}^k g L^k + K_p \rho_a^k\left(u^k\right)^2 \quad k = 1 \text{ to } 6 \tag{12}$$

where K_p is the flow coefficient of the air distributor, which is function of the design and geometry of the perforated plate [15]. The fluidization air total mass flowrates are assumed to be constant.

2.2. Population balance

The PBE solution allows calculating a distribution function that completely characterizes the PSD of the solid stream that exit each chamber [12,23]. Considering the particles diameter Dp as the internal coordinate, the unsteady-state PBE for a well-mixed granulation chamber, where only growth occurs, is:

$$\frac{\partial n}{\partial t} + G\frac{\partial n}{\partial Dp} = \dot{n}_{in} - \dot{n}_{out} \tag{13}$$

being G the growth rate (independent of the selected particle size) and $\dot{n}_{in}$ and $\dot{n}_{out}$ the number density function flows in and out of the system, respectively.

To solve the PBE, there is a variety of numerical methods [24–27]. One of the most popular is that proposed by Hounslow et al. [25] mainly because: its simple implementation, guarantees the correct prediction of the rate of change for the first three moments based on particle diameters (i.e., total particle number, length and surface [12]) and allows representing the volume or mass rate of change within acceptable errors. By applying the Hounslow discretization method, Eq. 13 becomes:

$$\frac{dN_i^k}{dt} = \frac{G^k}{Dp_i}\left(aN_{i-1}^k + bN_i^k + cN_{i+1}^k\right) + \dot{N}_{in\ i}^k - \dot{N}_i^k \quad i = 1 \text{ to } M \tag{14}$$

where N_i^k is the number of particles of size class i within chamber k and $\dot{N}_{in\,i}^k$ and $\dot{N}_i^k$ are the number flow of particles of size class i in and out of chamber k, respectively. M represents the number of size classes while a, b and c are constants whose values have been computed to predict correctly the changes in moments 0, 1 and 2 [25]:

$$a = \frac{2r}{(1+r)(r^2-1)} \quad b = \frac{2}{(1+r)} \quad c = -\frac{2r}{(1+r)(r^2-1)} \tag{15}$$

being r the ratio of the upper and lower limits for any size interval of a geometric grid ($r = Dp_{i+1}/Dp_i$).

Since the chamber is supposed to be perfectly mixed, the PSD of the solids outlet stream can be considered equal to the PSD inside the chamber; therefore the following relationship is satisfied:

$$\frac{\dot{N}_i^k}{\dot{m}_{out}^k} = \frac{N_i^k}{m_T^k} \tag{16}$$

By replacing Eqs. 15 and 16 in Eq. 14 the discretized PBE becomes:

$$\frac{dN_i^k}{dt} = \frac{G^k}{Dp_i}\left(aN_{i-1}^k + bN_i^k + cN_{i+1}^k\right) + \dot{N}_{in\ i}^k - \frac{\dot{m}_{out}^k}{m_T^k}N_i^k \quad i = 1 \text{ to } M \tag{17}$$

The PSD of each chamber is estimated as a function of time, solving the M ODEs defined by Eq. 17 and the following initial condition:

$$N_i^k(0) = N_{i\ 0}^k \quad i = 1 \text{ to } M \tag{18}$$

where $N^k_{i\,0}$ is the particles number in size class i within chamber k at $t=0$.

The particle growth rate (G^k) in Eq. 17 is the rate of increase in particle diameter resulting from the deposition of the tiny urea droplets on the particles surface. Assuming that particles belonging to different interval sizes grow proportional to its fractional surface area [3,15], G^k results:

$$G^k = \frac{dDp}{dt} = \frac{2\dot{m}^k_{melt}\left(1-x^k_{melt}\right)}{\rho_p Ap^k_T} = \frac{\dot{m}^k_{melt}\left(1-x^k_{melt}\right)Dp^k_{sv}}{3m^k_T} \tag{19}$$

where Ap_T and Dp^k_{sv} denote the total particles superficial area and surface-volume mean diameter within chamber k, respectively. This equation states that all the particles, independently of their sizes, grow at the same rate.

Eq. 19 can be rewritten in a discretized form:

$$G^k = G^k_i = \frac{2\dot{m}^k_{melt}\left(1-x^k_{melt}\right)}{\rho_p \pi \sum_i N^k_i \overline{Dp^2_i}} \tag{20}$$

where G^k_i is the growth rate of the particles being in the ith size interval and $\overline{Dp^2_i}$ is the mean size of class i that guarantees the second moment conservation [25].

The numerical solution of Eq. 17 together with the complementary expressions Eqs. 18 and 20 gives the dynamic evolution of the PSD within each granulator chamber. The solution must represent accurately the rate of change of moment 3, which is of particular interest here. The discretized moments are calculated as follows:

$$m^k_j = \sum_{i=1}^{M} \overline{Dp^j_i} N^k_i \tag{21}$$

where $\overline{Dp^j_i}$ is the mean size class i that ensures satisfying the jth moment [25]:

$$\overline{Dp^j_i} = \frac{1}{j+1}\left(\frac{r^{j+1}-1}{r-1}\right)Dp^j_i \tag{22}$$

For the described granulation unit, the rate of change of moments 0 and 3 are:

$$\frac{dm^k_0}{dt} = \frac{dN^k_T}{dt} = \dot{N}^k_{in} - \dot{N}^k_{out} = \dot{N}^k_{in} - \frac{\dot{m}^k_{out}}{m^k_T} N^k_T \tag{23}$$

$$\frac{dm^k_3}{dt} = \frac{dm^k_T}{dt} = \dot{m}^k_{in} + \dot{m}^k_{melt}\left(1-x^k_{melt}\right) - \dot{m}^k_{out} \tag{24}$$

where N^k_T is the total number of particles within chamber k. From Eqs. 23 and 24, the values of the moments 0 and 3 as a function of time can be precisely calculated and compared with the moments obtained by using Eq. 21 and the PSD estimated through the discretized PBE to establish the accuracy of the numerical solution.

2.3. SGN and UI for a log-normal distribution

Two parameters are commonly used in the fertilizers industry to define the product quality. The Size Guide Number (SGN) is the median (Dp_{50}) in millimeters of the mass size distribution, multiplied by 100. In other words, the SGN is defined as the particle size in millimeters for which 50% by weight of the sample is coarser and 50% finer times 100. The uniformity index (UI) characterizes the spread of the product PSD and is defined as the ratio of the opening size that would let pass 5 wt.% of the corresponding sample to the opening that would let pass 90 wt.%, multiplied by 100.

The granular urea particle size distributions are skewed to the right, as many other particulate systems. Therefore, the log-normal distribution becomes a good representation for particle populations of this fertilizer [28]. If the PSD is characterized as log-normal, then the SGN can be expressed as follows [29]:

$$SGN = 100\mu_g \tag{25}$$

where μ_g is the geometric mean diameter of the mass PSD in mm.

On the other hand, UI is given by:

$$UI = 100\sigma_g^{-2.926} \tag{26}$$

where σ_g is the geometric standard deviation of the PSD in mm. The derivation of Eq. 26 is presented in Appendix. Thus, the parameters SGN and UI can be calculated from the geometric mean diameter and standard deviation of the PSD expressed in mass weight percent.

To find theoretical equations for the prediction of μ_g and σ_g, the PBE (Eq. 13) is rewritten defining $w = \frac{\rho_p \pi n Dp^3}{6m_T}$ as the normalized mass density function. Considering the w definition and Eq. 19, Eq. 13 becomes:

$$m_T\frac{\partial w}{\partial t} + w\frac{\partial m_T}{\partial t} + \frac{\dot{m}_{melt}\left(1-x^k_{melt}\right)Dp_{sv}}{3}\frac{\partial w}{\partial D_p} - \dot{m}_{melt}Dp_{sv}\frac{w}{Dp} = \dot{m}_{in}w_{in} - \dot{m}_{out}w \tag{27}$$

For each chamber, the geometric mass mean μ_g and standard deviation σ_g are:

$$\ln\mu^k_g = \int_0^\infty w^k \ln Dp dDp \tag{28}$$

$$\ln^2\sigma^k_g = \int_0^\infty w^k\left(\ln Dp - \ln\mu^k_g\right)^2 dDp \tag{29}$$

Multiplying Eq. 27 by $\ln Dp$, integrating over the whole particles size domain and considering a log-normal PSD, the following differential equation is obtained to estimate the evolution of μ_g with time:

$$m^k_T\frac{d\mu^k_z}{\partial t} = \dot{m}^k_{melt}\left(1-x^k_{melt}\right)\left[\frac{1}{3} - \left(\sigma^k_z\right)^2\right] + \dot{m}^k_{in}\left(\mu^k_{z\,in} - \mu^k_z\right) \tag{30}$$

where $\mu^k_z = \ln\mu^k_g$ and $\sigma^k_z = \ln\sigma^k_g$.

To predict the rate of change of the geometric standard deviation for a log-normal PSD, Eq. 27 is multiplied by $\left(\ln Dp - \ln\mu^k_g\right)^2$ and integrated over the whole particles size domain.

$$m_T\frac{d\left(\sigma^k_z\right)^2}{dt} = \dot{m}_{melt}\left(1-x^k_{melt}\right)\left(\sigma^k_z\right)^4 - \frac{2}{3}\dot{m}_{melt}\left(1-x^k_{melt}\right)\left(\sigma^k_z\right)^2 + \dot{m}_{in}\left[\left(\sigma^k_{z\,in}\right)^2 - \left(\sigma^k_z\right)^2\right] + \dot{m}_{in}\left(\mu^k_{z\,in} - \mu^k_z\right)^2 \tag{31}$$

Eqs. 30 and 31 allow calculating μ^k_g and σ^k_g as a function of the inlet solids and melt mass flowrates, the solids' holdups within chamber and the geometric mean and standard deviation of the PSD that enters into chamber k.

Therefore, the steady-state *SGN* and *UI* can be computed from Eqs. 30 and 31 as follows:

$$\mu_{z\,in}^{k}-\mu_{z}^{k}=\frac{\dot{m}_{melt}^{k}\left(1-x_{melt}^{k}\right)}{\dot{m}_{in}^{k}}\left[\left(\sigma_{z}^{k}\right)^{2}-\frac{1}{3}\right] \tag{32}$$

$$\left(\sigma_{z}^{k}\right)^{4}-\frac{2}{3}\left(\sigma_{z}^{k}\right)^{2}+\frac{\dot{m}_{in}^{k}}{\dot{m}_{melt}^{k}\left(1-x_{melt}^{k}\right)}\left(\left(\sigma_{z\,in}^{k}\right)^{2}-\left(\sigma_{z}^{k}\right)^{2}\right) + \frac{\dot{m}_{in}^{k}}{\dot{m}_{melt}^{k}\left(1-x_{melt}^{k}\right)}\left(\mu_{z\,in}^{k}-\mu_{z}^{k}\right)^{2}=0 \tag{33}$$

The *SGN* and *UI* values estimated by means of Eqs. 32 and 33 (which are derived from the continuous PBE and a log-normal particle size distribution) are compared to *SGN* and *UI* predicted by the discretized PBE in Section 3.2.

2.4. Numerical solution

The model is solved using the FORTRAN programming language. The set of ordinary differential equations constituted by Eqs. 1, 9 and 17 is simultaneously integrated by means of a Gear subroutine to estimate the solids mass, bed temperature and number of particles per class for all the chambers. The fluidized beds porosity, height and pressure drop, the growth rate and the solids' flow leaving each chamber, among other variables, are also computed at every time interval.

The population balance is solved for a geometric grid of ratio $r=2^{1/6}$ and the entire size range is divided in 45 intervals ($M=45$). The seeds' PSD is modelled as a log-normal distribution and discretized to obtain the number of particles per class *i*.

3. Simulation results and discussion

The simulation results are discussed in the following two sections. First, the steady-state results for a given set of operating conditions specified to define a base case are presented. The corresponding variables are selected from typical industrial values of a continuous fluidized bed granulator for urea production [6]. In the second section, different step changes are imposed around the steady-state values of the base case in order to analyze the dynamic responses of the product granulometry and to explore the stability of the granulator outlet PSD against changes in key operating variables.

3.1. Steady-state. Base case

Fig. 2 shows, for the base case, steady-state simulation results for all the chambers. The variables are dimensionless; they are referred to the values corresponding to the first chamber. For the given granulometry and mass flowrate of the seeds, fluidization air velocity, melt flowrate, cross sectional area of each chamber and passage and discharge areas, the mass balances (Eqs. 1 to 8) allow calculating the solids' holdups as shown in Fig. 2a. The particles' number profile, which is also presented in Fig. 2a, is related to the solid mass and PSD within each chamber. Since the mass holdups within chambers 1 to 3 are almost equal and the particles grow along these three growth chambers, the total particles' number decreases from chambers 1 to 3. On the other hand, in the last three fluidized beds, the particles' number decreases according to the observed solids mass diminution.

As indicated by Eqs. 8 and 12, the factor $L^{k}\,\rho_{bed}^{k}$ (shown in Fig. 2b) is proportional to the m_T^k/A_T^k ratio and to the hydrostatic pressure in the fluidized bed, respectively. The chambers cross sectional areas and the passage and discharge areas are carefully selected to guarantee a decreasing profile for $L\rho_{bed}$, which is the driven force for the solids' flow in the horizontal direction towards the granulator outlet (Eq. 3). The bed heights, also shown in Fig. 2b, follow the trend exhibited by the bed porosities (data not shown), which are dependent on the superficial air velocity profile and the population PSD within each chamber.

For all the chambers, the fluidized bed temperatures are presented in Fig. 2c. The bed temperatures of the three first chambers are higher than those of the last three ones, basically due to the melt addition that is sprayed at high temperature (about 132 °C [29,30]) in chambers 1 to 3. The bed temperature of chamber 1 is lower than those corresponding to the other growth chambers because the recycled seeds enter at a relatively low temperature (around 60 °C). Fig. 2c also shows the total pressure drop for each chamber. Considering Eq. 12 and the $L\rho_{bed}$ profile presented in Fig. 2b, it can be concluded that the air distributor is important in the estimation of the total pressure drop within each chamber.

Fig. 2d shows the solids' flow that leaves each chamber on mass and number basis. The solids mass flow increases from chambers 1 to 3 due the melt addition and then remains constant up to the granulator outlet because no melt is fed in chambers 4 to 6 (Eq. 1). The steady-state particles number flows are equal for all the chambers, satisfying the only growth mechanism imposed to the particles (Eq. 23).

For the base operating conditions and all the granulator chambers, the steady-state particle size distributions are shown in Fig. 3. In Fig. 3a, the PSDs are expressed in normalized number frequency distributions. The degree of mixing within the granulator has an important effect on the granule size distribution. The PSD greatly broadened from the seeds' (inlet) size distribution as a consequence of the exponential residence time distribution of the particles in each well-mixed fluidized growth chamber [3]. The PSDs of chambers 4 to 6 are identical to that of chamber 3, as expected from Eq. 14 for steady-state and null growth rate.

For the base case, moments 0 and 3 are satisfactorily predicted with errors lower than 10^{-3} and 0.3%, respectively.

In Fig. 3b the PSDs are expressed in mass because sieving is the most common method of size analysis in the industrial practice. For these calculated PSDs, Table 1 summarizes the *SGN* and *UI* values. The *SGN* gradually increases from the inlet to chamber 3 and then remains constant up to the granulator outlet. For this base case, the product *SGN* and *UI* are 15% and 34% higher than those of the seeds, respectively. The *SGN* and *UI* predicted by Eqs. 32 and 33 differ from those reported in Table 1 in less than 0.35 and 1.9%, respectively. These low values indicate that the PSDs can be satisfactorily described by log-normal distribution functions.

For the proposed model, the calculation of the steady-state variables (such as bed heights, chamber temperatures, total pressure drops and mass holdups) requires a good prediction of the bed porosity, which is a function of the PSD. The hydrodynamic properties could be estimated without the solving the PBE by means of the number-volume mean diameter Dp_{nv}, which can be computed for each chamber using the following Eq. [10]:

$$\frac{dDp_{nv}^{k}}{dt}=\frac{Dp_{nv}^{k}}{3m_{T}^{k}}\left[\dot{m}_{in}^{k}\left[1-\left(Dp_{nv}^{k}\Big/Dp_{nv}^{k-1}\right)^{3}\right]+\dot{m}_{melt}^{k}\left(1-x_{L}^{k}\right)\right] \tag{34}$$

However, the hydrodynamic properties should be evaluated by using the surface-volume mean diameter Dp_{sv}[31,32].

Fig. 4 shows for each chamber the Dp_{nv} and Dp_{sv}values, which differ in about 20%. The differences between these two mean sizes lead to significant differences in the prediction of the bed heights, pressure drops and solids' holdups. For example, errors around 30% are found in the calculation of the bed heights without using the PBE. Even though the use of Dp_{nv} does not introduce errors in the bed temperatures estimations (in agreement with the model hypothesis), there is a need to couple the PBE to the mass, energy and momentum balances for a reliable prediction of the absolute values of the main granulator variables. However, it is important to note that the use of

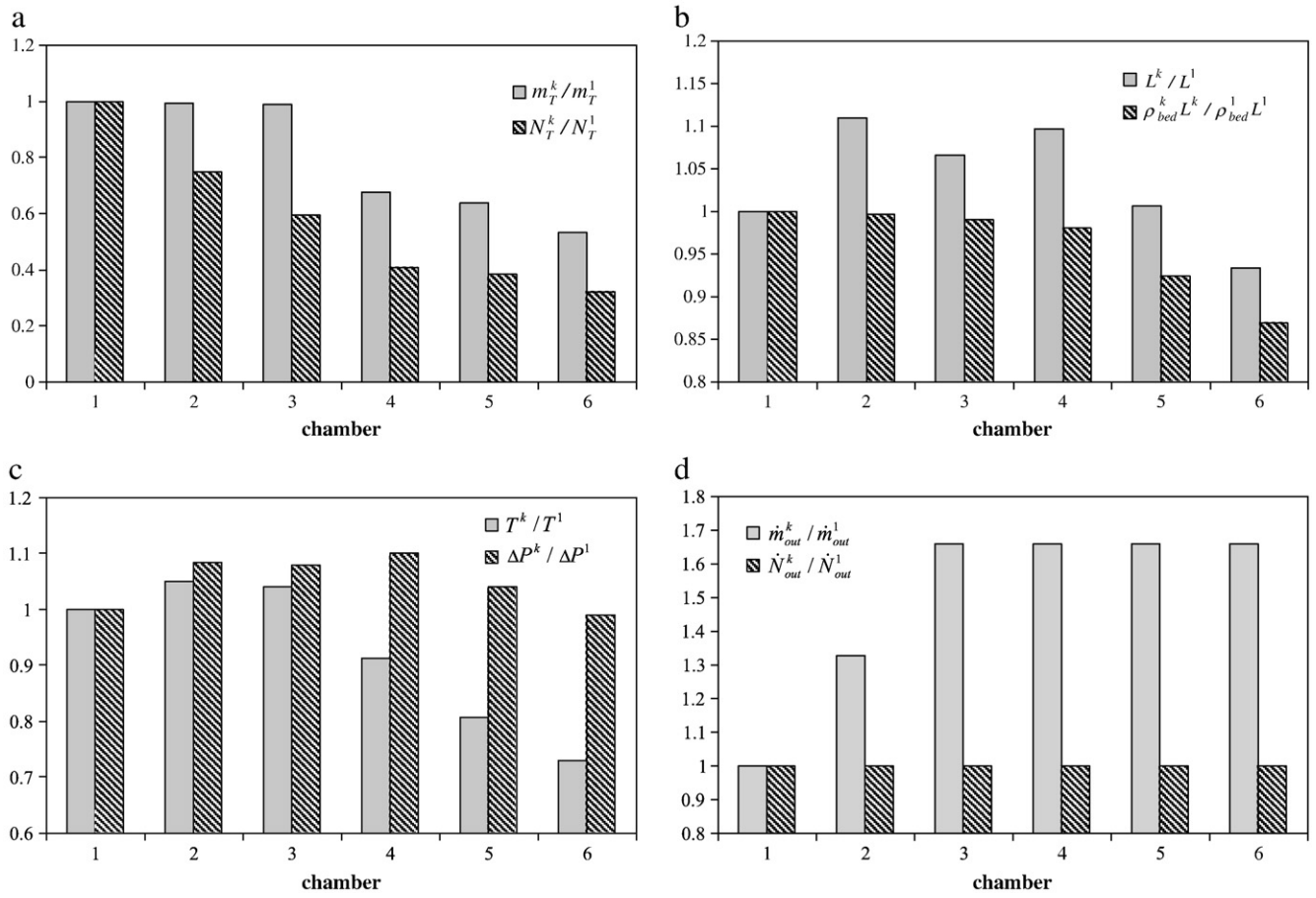

Fig. 2. Dimensionless steady-state simulation results for the base case.

Dp_{nv} allows well predicting the dynamic and steady-state trends of the state variables. The differences between Dp_{nv} and Dp_{sv} are higher as the particle size distributions get broader. In fact, Dp_{sv}/Dp_{nv} ratios lower than 1 and 5% are calculated for PSDs with *UI* values higher than 75 and 52, respectively.

3.2. Sensitivity analysis and dynamic simulation

In early works [10,11], the open-loop behaviour of the state variables was analyzed by means of the momentum, mass and energy balances. The bed heights, pressure drops, solids' holdups and mass flows were the most sensible to changes in the seeds' mass flowrates, total fluidization air mass flows and discharge area, exhibiting long dynamic transition times (in concordance with the high capacity of the simulated industrial unit). The bed temperatures and porosities presented faster dynamics and were less influenced by the disturbances assayed in the inlet conditions. The product discharge area, fluidization air temperature and flowrates were identified as the more appropriate manipulative variables to respectively control the bed height, temperature and porosity.

The previous results of the open-loop behaviour analysis are confirmed by the simulations performed coupling the PBE to the fundamental granulator balances. In this study, special attention is focused on the open-loop behaviour of the product PSD. To this end, the granulator is subjected to +10% step disturbances in the seeds' *SGN* and *UI* as well as in the seeds and melt flowrates (which are the only inlet variables that cause changes in the final steady-state granulometry).

Fig. 5 presents for the last granulator chamber, the transient profiles of the bed height, mass holdup, total pressure drop, solids mass flow and bed temperature against a +10% step change in the seeds' mass flowrate (performed after 10 min under steady-state operation) obtained by means of the granulator model with and without the PBE. As it can be seen, the PBE is an indispensable statement of continuity not only to predict the product granulometry but also to accurately estimate the main granulator state variables.

Fig. 6 shows the product *SGN* and *UI* at the final steady-state (expressed as a percentage of the corresponding initial steady-state value) for the abovementioned step disturbances, imposed one at a time. These two parameters were calculated by means of both, the microscopic (Eq. 17) and macroscopic (Eqs. 25, 26, 32 and 33) PBEs. For the +10% change in the seeds' *SGN*, the new steady-state value indicates a direct proportional change in the product mass median. This result is in perfect agreement with the steady-state geometric mean and standard deviation theoretically derived for a log-normal distribution (Eqs. 32 and 33). In fact if $\dot{m}_{in}$, $\dot{m}_{melt}$, x_{melt} and $\sigma_{z\ in}$ are specified, σ_z is fixed and thus the geometric mean at each chamber outlet results directly proportional to its inlet value. With respect to the product *UI*, the +10% step change in seeds' *UI* produces the highest impact. The effect of the seeds' *SGN* on the product *UI* is almost negligible, in agreement with Eqs. 32 and 33 which show that the product *UI* is independent of the seed *SGN* for log-normal distributions. The small differences between the results obtained from the microscopic and macroscopic PBEs may be attributed to PSDs inside the chambers not exactly log-normal. Regarding the disturbances assayed in seeds and melt flowrate, the 10% positive steps have opposite effects on the particles growth rate and consequently on the product *SGN* deviations. Fig. 6 indicates that in order to maintain the product *SGN*, the $\dot{m}_{in}/\dot{m}_{melt}$ ratio (which is strongly related to the recycle ratio of industrial granulation plants) should be significantly

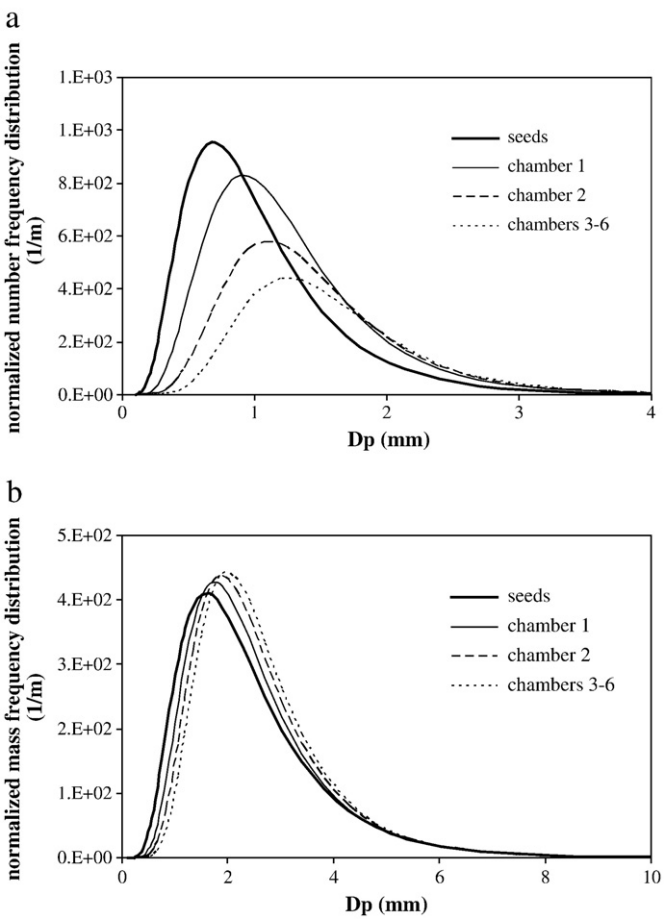

Fig. 3. PSD curves expressed in normalized number frequency distribution (a) and in normalized mass frequency distribution (b).

modified to compensate the fluctuations in the seeds' *SGN* and *UI*. The recycle ratio is not a recommendable variable to hold the spread of the product PSD constant.

Fig. 7 presents the evolution of the product *SGN* over time for +10% step changes in the seeds' *SGN* and *UI* (performed at t = 10). The high capacity industrial granulator requires about 1 h to reach the new steady-state granulometry. These large response times considerably affect the dynamics of the whole granulation circuit and justify the common assumption of pseudo-steady-state for the modeling of the screening and crushing units [33].

Changes in the granulator outlet PSD have a significant impact on the recycle ratio R and vice versa. To explore the influence of the product PSD on the granulation circuit stability, the effect of the recycle ratio defined as the relationship between the seeds and total melt flowrates (i.e., for an even melt distribution along the growth chambers, the recycle ratio results equal to $\dot{m}_{in} / 3\dot{m}_{melt}(1-x_L^k)$) is analyzed. Fig. 8 shows the steady-state product *SGN* as a function of the recycle ratio, for a given seeds' PSD (the one of the base case). As the recycle ratio increases, the *SGN* decreases monotonically tending to that of the seeds for extremely large recycle ratios. For a specified plant capacity (i.e., constant melt flowrate), an increment in the seeds' mass flowrate (i.e., in the recycle ratio) results

Table 1
SGN and *UI* for each chamber in the base case.

	Seeds	Chamber 1	Chamber 2	Chambers 3–6
SGN	211.3	221.0	230.6	239.8
UI	21.1	24.5	27.1	29.0

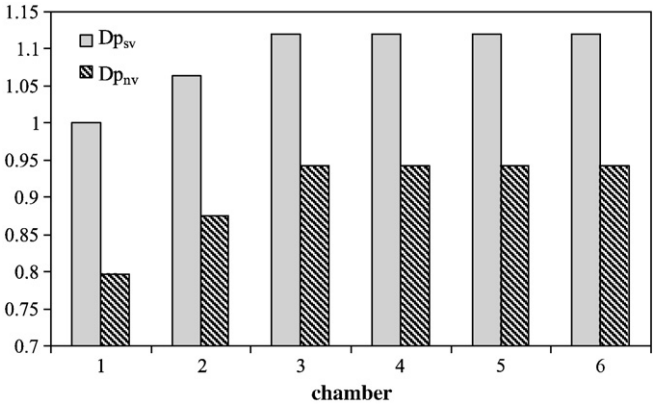

Fig. 4. Dimensionless number-volume and surface-volume mean steady-state diameters for the base case.

in a higher residence time because the increase in the granulator mass holdup is more important than that in the outlet solids mass flowrate (e.g., see in Fig. 5 the changes in m_T and m_{out}^6 between the final and initial steady-states for a +10% step change in the seeds' mass flowrate). On the other hand and according to Eq. 19, the particles growth rate (which is inversely proportional to the mass holdup) decreases with increments in the seeds' mass flowrate. The net particles growth, given by the product of the residence time and the particles growth rate, diminishes as the seeds' mass flowrate increases basically because the change in the particles growth rate is higher than that in the residence time. Consequently, the product mean size (*SGN*) diminishes as the recycle ratio increases. As it can be seen in Fig. 8, the slope of the product *SGN* decreases as a function of the recycle ratio. Therefore, large recycle ratios tend to attenuate the changes in the granulator outlet PSD stabilizing the granulation circuit operation. However, the recycle ratios are limited in the industrial practice by the nominal capacities of the units and the marketable product *SGN*. The *SGN* of the solids stream that leaves the granulator has to be within the range determined by the seeds' *SGN* and the final product SGN (about 300 [34]). In fact, if a granulator outlet *SGN* higher than 230 are desired, the granulator must operate with recycle ratios lower than approximately 0.55.

The recycle ratios may not only attempt on the marketable product *SGN* but also on the good operability of the granulator. Among other granulator state variables, the chambers temperature becomes essential to guarantee the melt granulator operation stability and product quality. For this reason and with the aim of identifying the feasible recycle ratio

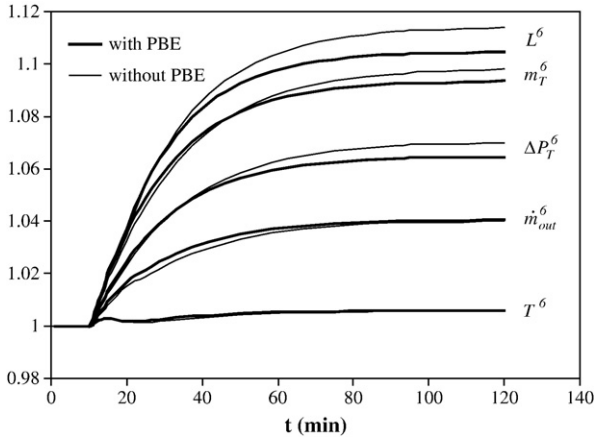

Fig. 5. Dimensionless transient profiles of the last chamber bed height, mass holdup, total pressure drop, solids mass flow and bed temperature against a +10% step change in the seeds' mass flowrate for the granulator model with and without PBE.

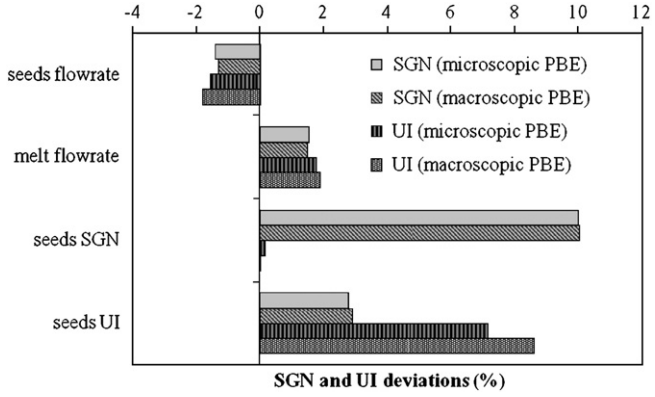

Fig. 6. Changes in the product *SGN* and *UI* against the + 10% step disturbances assayed in different inlet granulator variables, calculated by means of both the microscopic (Eq. 17) and macroscopic (Eqs. 25, 26, 32 and 33) PBEs.

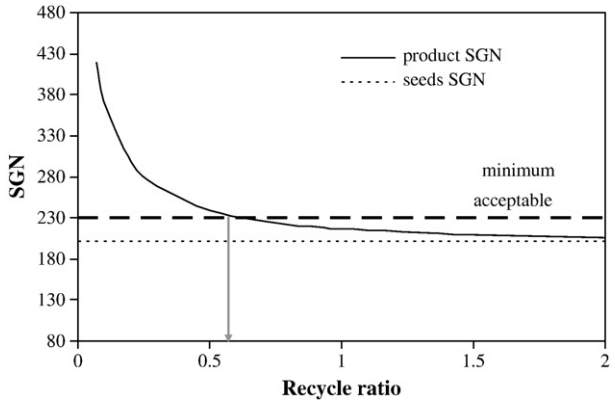

Fig. 8. Product *SGN* as a function of the recycle ratio $\dot{m}_{in} / 3\dot{m}_{melt}(1-x^k_{melt})$.

range, the effect of the seeds' mass flowrate on the bed temperatures of the growth chambers is also analyzed. Fig. 9 presents the growth chambers temperature as a function of the recycle ratio, for the seeds' PSD given in the base case. As the recycle ratio increases, the growth chambers temperature decreases and the maximum granulator temperature shifts from the first to the last growth chamber. The thermal condition of the growth chambers limits the recycle operating range of the industrial granulators for urea production. The bed temperatures have to remain high (not lower than 100 °C, [6]) in order to avoid the melt solidification in the spray nozzles but should not be close to the melting point (about 132 °C, [6]) because this would lead to partial or total quenching of the bed. According to Fig. 9, the recycle ratio has to be between 0.25 and 1.5 to ensure growth chamber temperatures within the required range.

Consequently, for a given seeds' PSD, the recycle ratio values (0.55–1.5) are constrained by the minimum acceptable product *SGN* and the maximum allowable bed temperature.

Considering that the seeds' *SGN* depends on the granulation circuit performance and that the urea melt feed is defined by the specified plant capacity, these two variables cannot be usually manipulated. Therefore, the only variable that can be used to control the granules size is the seeds' mass flow. Since the seeds are a recycle stream, a fresh seeds' storage system and/or recycle stream bypass would be required to make possible the suggested product size control. The feasibility of this approach cannot be evaluated with the presented granulator dynamic model. To this end, the simulation of the whole urea granulation circuit results necessary.

4. Conclusions

A complete dynamic model of a continuous multichamber industrial fluidized bed granulator for urea production is presented. Mass, energy and momentum balances are solved for all the fluidized beds together with the population balance equation. Based on the PBE, the continuous rate of change of the geometric mass mean and standard deviation (assuming the PSD within each chamber are well described by log-normal functions) are theoretically derived.

The PBE is found to be an indispensable statement of continuity to accurately estimate the main granulator state variables excepting the bed temperature. The number-volume mean diameter of the population, which can be calculated without solving the PBE, is a good representation of the surface-volume mean diameter just for relatively narrow particle size distributions. For these situations only, the number-volume mean diameter allows well predicting the granulation unit performance.

The log-normal distribution function is found to be an appropriate description of the granulometry for the seeds' and particles' populations within each chamber. The use of the continuous rate of change of the geometric mean and standard deviation (theoretically derived) allows tracking accurately the PSDs along the granulator. Therefore, this approach can substitute the use of the PBE without introducing significant errors.

The product granulometry shows low response times, indicating that the granulation unit would control the dynamics of the whole circuit. The seeds' PSD is the variable that most affect the outlet particle size distribution, being then important to make attempts to maintain the granular product quality. This result strongly suggests

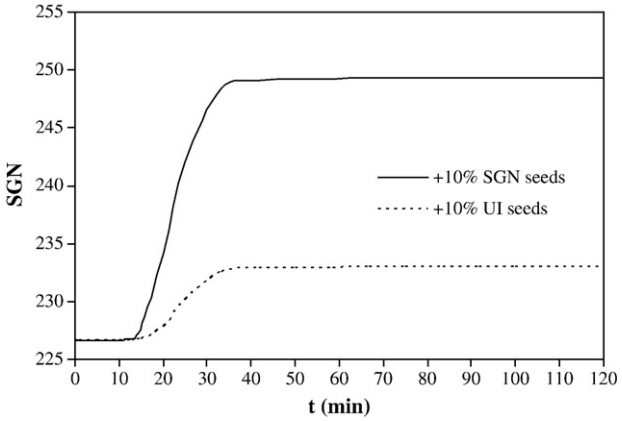

Fig. 7. Dynamic evolution of the product *SGN* for the + 10% step disturbances assayed in the seeds' *SGN* and *UI* at t = 10 min.

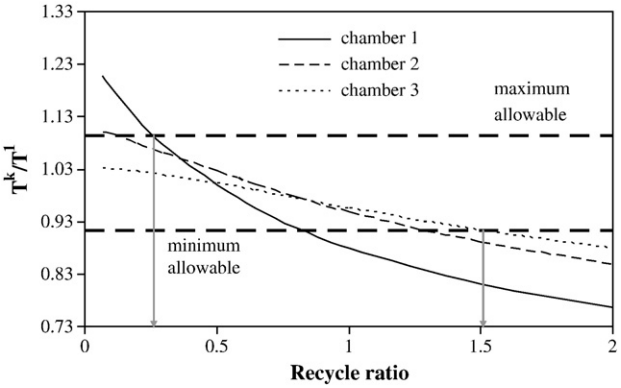

Fig. 9. Dimensionless growth chambers temperature as a function of the recycle ratio $\dot{m}_{in} / 3\,\dot{m}_{melt}(1-x^k_{melt})$.

the need of exploring different granulation circuit flowsheets aiming to keep the seeds' granulometry close to the desired size distribution.

Besides, for a given seeds' PSD, mild recycle ratio values are found as adequate to stabilize the granulator operations. Large recycle ratios tend to attenuate the changes in the granulator outlet PSD, while low values may lead to melt quenching of the bed.

The coupling of the PBE to the momentum, mass and energy balances of the urea multichamber fluidized bed granulator allowed complementing the open-loop behaviour analysis previously performed. Further research will be focused on the closed-loop behaviour of the industrial granulator, with the aim of improving its operability.

Acknowledgments

The authors gratefully acknowledge the financial support by the Consejo Nacional de Investigaciones Científicas y Técnicas (CONICET), the Agencia Nacional de Promoción Científica y Tecnológica (ANPCyT) and the Universidad Nacional del Sur (UNS) from Argentina.

Nomenclature

a	constant in the discretized growth term proposed by Hounslow [−].
A	superficial area [m^2].
A_o	passage or discharge area [m^2].
A_T	total cross sectional area [m^2].
b	constant in the discretized growth term proposed by Hounslow [−].
c	constant in the discretized growth term proposed by Hounslow [−].
C_D	solid discharge coefficient [−].
cp	mass heat capacity [J/Kg K].
Dp	particle diameter [m].
Dp_5	opening size that would let pass 5 wt.% of the particles sample [m].
Dp_{50}	median of the mass particle size distribution [m].
Dp_{90}	opening size that would let pass 90 wt.% of the particles sample [m].
$\overline{Dp_i^j}$	mean size of class i that guarantees the conservation of moment jth [m].
g	gravity acceleration [m/s^2].
F	cumulative mass distribution [−].
G	growth rate [m/s].
K_P	flow coefficient for the perforated plate (Eq. 12) [−].
K_ε	exponent in Eq. (6) [−].
L	fluidized bed height [m].
m	bed mass [Kg].
m_j	jth moment of the distribution [m^j].
$\dot{m}$	mass flowrate [Kg/s].
M	number of size classes [−].
n	number frequency distribution [#/m].
$\dot{n}$	number frequency distribution per unit time [#/m s].
N	particles number [#].
$\dot{N}$	particles number flowrate [#/s].
r	ratio of the upper and lower limit sizes in a interval of a geometric grid [−].
R	$\dot{m}_{in}$ / $3\dot{m}_{melt}$, recycle ratio [−].
SGN	size guide number [−].
t	time [s].
T	temperature [°C].
u	superficial air velocity [m/s].
u_t	particle terminal velocity [m/s].
UI	uniformity index [−].
x	solution water content, wet basis [$Kg_{water}/Kg_{solution}$].
Y	mass air humidity, dry basis [$Kg_{water}/Kg_{dry\ air}$].
w	normalized mass density function [1/m].

Greek symbols

ΔH	latent heat [J/Kg].
ΔP	pressure drop [Pa].
ε	bed void fraction [m^3_{air}/m^3_{bed}].
μ_g	geometric mean diameter [mm].
μ_z	logarithm of μ_g [−].
ρ	density [Kg/m^3].
σ_g	geometric standard deviation [mm].
σ_z	logarithm of σ_g [−].

Subscripts

0	initial.
a	atomization and fluidization dry air.
bed	fluidized bed.
DIS	dissolution.
$dist$	at the distributor.
EV	evaporated water.
g	geometric.
i	size class.
in	inlet.
$melt$	urea melt.
mf	at minimum fluidizing conditions.
nv	number-volume.
out	outlet.
p	particles.
sv	surface-volume.
T	total.
u	solid urea.
v	vapor.
w	water.

Superscripts

k	chamber number.

Appendix A

The UI is defined as:

$$UI = 100\,\frac{Dp_5}{Dp_{90}} \tag{A1}$$

where Dp_5 and Dp_{90} are the particle diameters that respectively satisfy:

$$F(Dp_5) = 0.05 \tag{A2}$$

$$F(Dp_{90}) = 0.9 \tag{A3}$$

being $F(Dp)$ the normalized cumulative mass distribution, which for a log-normal function can be written as:

$$\frac{1}{2}\left[erf\left(\frac{\ln Dp - \ln \mu_g}{\sqrt{2}\ \ln \sigma_g}\right) + 1\right] = F(Dp) \tag{A4}$$

Evaluating Eq. A4 for F equal to 0.05 and 0.9, Dp_5 and Dp_{90}become:

$$Dp_5 = \mu_g\, e^{-1.163\sqrt{2}\ \ln\sigma_g} = \mu_g\, \sigma_g^{-1.645} \tag{A5}$$

$$Dp_{90} = \mu_g\, e^{0.906\sqrt{2}\ \ln\sigma_g} = \mu_g\, \sigma_g^{1.282} \tag{A6}$$

By replacing Eqs. A5 and A6 in Eq. A1, the uniformity index as a function of the geometric standard deviation results:

$$UI = 100\,\sigma_g^{-2.926} \tag{A7}$$

References

[1] Fertilizer Manual, United Nations Industrial Development Organization (UNIDO) and International Fertilizer Development Center (IFDC), Kluwer Academic Publishers, The Netherlands, 1998.
[2] P. Heffer, M. Prud'homme, World agriculture and Fertilizer Demand, Global Fertilizer Supply and Trade. Summary Report, International Fertilizer Industry Association (IFA), 34th IFA Enlarged Council Meeting, Ho Chi Minh City, Vietnam, 2008.
[3] J. Litster, B. Ennis, L. Liu, The Science and Engineering of Granulation Processes. Particle Technology Series, Dordrecht, Kluwer Academic Publishers, 2004.
[4] P. Knight, Challenges in granulation technology, Powder Technology 130 (2004) 156–162.
[5] F.Y. Wang, I.T. Cameron, A multi-form modelling approach to the dynamics and control of drum granulation processes, Powder Technology 179 (2007) 2–11.
[6] A.F. Kayaert, R.A.C. Antonus, Process for the production of urea granules, US Patent 5 (653) (1997) 781.
[7] K.Y. Fung, K.M. Ng, S. Nakajima, C. Wibowo, A systematic iterative procedure for determining granulator operating parameters, AIChE Journal 52 (9) (2006) 3189–3202.
[8] I.T. Cameron, F.Y. Wang, C.D. Immanuel, F. Stepanek, Process systems modelling and applications in granulation: a review, Chemical Engineering Science 60 (2005) 3723–3750.
[9] M. Hasltensen, P. de Bakker, K.H. Esbensen, Acoustic chemometric monitoring of an industrial granulation production process—a PAT feasibility study, Chemometrics and Intelligent Laboratory Systems 84 (2006) 88–97.
[10] D.E. Bertin, J. Piña, V. Bucalá, Dynamics of an industrial fluidized bed granulator for urea production, Industrial and Engineering Chemistry Research 49 (1) (2008) 317–326.
[11] D.E. Bertin, J. Piña, V. Bucalá, Modelo Dinámico de un Granulador Industrial de Lecho Fluidizado para la Producción de Urea, I Reunión Interdisciplinaria de Tecnología y Procesos Químicos, Córdoba, Argentina, 2008.
[12] K. Saleh, P. Guigon, Coating and encapsulation processes in powder technology, in: A.D. Salman, M.J. Hounslow, J.P.K. Seville (Eds.), Handbook of Powder Technology, Elsevier, Amsterdam: The Netherlands, 2007, pp. 323–375.
[13] A.E. Nienow, P.N. Rowe, Particle growth and coating in gas-fluidized beds, in: J.F. Davidson, R. Clift, D. Harrison (Eds.), Fluidization, 2nd ed., London, Academic Press, 1985, pp. 564–594.
[14] D.E. Bertín, G.D. Mazza, J. Piña, V. Bucalá, Modeling of an industrial fluidized bed granulator for urea production, Industrial and Engineering Chemistry Research 46 (2007) 7667–7676.
[15] L. Mörl, S. Heinrich, M. Peglow, Fluidized bed spray granulation, in: A.D. Salman, M.J. Hounslow, J.P.K. Seville (Eds.), Handbook of Powder Technology, Elsevier, Amsterdam: The Netherlands, 2007, pp. 21–188.
[16] L. Garnavi, N. Kasiri, S.H. Hashemabadi, Mathematical modeling of a continuous fluidized bed dryer, International Communications in Heat and Mass Transfer 33 (2006) 666–675.
[17] E. Grieco, L. Marmo, Predicting the pressure drop across the solids flow rate control device of a circulating fluidized bed, Powder Technology 161 (2006) 89–97.
[18] L. Massimilla, Flow properties of the fluidized dense phase, in: J.F. Davidson, D. Harrison (Eds.), Fluidization, New York, Academic Press, 1971, pp. 651–676.
[19] D.E. Bertin, J. Piña, G. Mazza, V. Bucalá, Modelado de un granulador de lecho fluidizado para la producción de urea granulada, XXI Interamerican Congress of Chemical Engineering, Buenos Aires, Argentina, 2006.
[20] D.E. Bertin, V. Bucalá, J. Piña, Dynamics and Control of an Industrial Fluidized Bed Granulator with Multiple Beds. Application to Urea Production. 10th International Chemical and Biological Engineering Conference, Braga, Portugal, 2008.
[21] T.E. Daubert, R.P. Danner, Thermodynamics Properties of Pure Chemicals: Data Compilation, Taylor & Francis, London, 1996.
[22] Kirk–Othmer Encyclopedia of Chemical Technology, Wiley, New York, 1991.
[23] A.D. Randolph, M.A. Larson, Theory of Particulate Process, Academic Press, New York, 1971.
[24] D. Ramkrishna, Population Balances: Theory and Applications to Particulate Systems in Engineering, Academic Press, San Diego, 2000.
[25] M.J. Hounslow, R.L. Ryall, V.R. Marshall, A discretized population balance for nucleation, growth and aggregation, AIChE Journal 34 (11) (1988) 1821–1832.
[26] M. Nicmanis, M.J. Hounslow, Finite-element methods for steady-state population balance Eq.s, AIChE Journal 44 (10) (1998) 2258–2272.
[27] S. Kumar, D. Ramkrishna, On the solution of population balance Eq.s by discretization-I. A fixed pivot techniqhe, Chemical Engineering Science 51 (8) (1996) 1311–1332.
[28] T. Allen, Powder Sampling and Particle Size Determination, Elsevier, Amsterdam: The Netherlands, 2003.
[29] P.J.B. Nijsten, P.J.M. Starmans, Process for producing granules, US Patent 5 (779) (1998) 945.
[30] A. Niks, W.H.P. Van Hijfte, R.A.J. Goethals, Process for urea granulation, US Patent 5 (653) (1997) 781.
[31] D. Kunii, O. Levenspiel, Fluidization Engineering, Butterworth-Heinemann, Boston, 1991.
[32] M. Rhodes, Introduction to Particles Technology, England, West Sussex, 1998.
[33] Wildeboer, W.J., 1998. Steady State and Dynamic Simulations of a Closed Loop Granulation Circuit, Masters Thesis, Delft University of Technology, Delft, The Netherlands.
[34] Karnaphuli Fertilizer Company Limited, Rangadia, Anowara Chittagong, Bangladesh, http://www.kafcobd.com/html/products.html.